PL-TR-94-2152

AD-A283 239

SEISMIC STUDIES OF THE CASPIAN BASIN AND SURROUNDING REGIONS

DTIC
ELECTE
JUL 15 1994
S D
F

Stephen Mangino
Keith Priestley

Department of Earth Sciences
University of Cambridge
Cambridge CB3 0EZ
UK

94-21504

14 May 1994

Scientific Report No. 1

DTIC QUALITY INSPECTED 8

APPROVED FOR PUBLIC RELEASE; DISTRIBUTION UNLIMITED

PHILLIPS LABORATORY
Directorate of Geophysics
AIR FORCE MATERIEL COMMAND
HANSCOM AFB, MA 01731-3010

94 7 12 100

The views and conclusions contained in this document are those of the authors and should not be interpreted as representing the official policies, either express or implied, of the Air Force or the U.S. Government.

This technical report has been reviewed and is approved for publication.

JAMES F. LEWKOWICZ
Contract Manager
Earth Sciences Division

JAMES F. LEWKOWICZ, Director
Earth Sciences Division

This report has been reviewed by the ESC Public Affairs Office (PA) and is releasable to the National Technical Information Service (NTIS).

Qualified requestors may obtain additional copies from the Defense Technical Information Center. All others should apply to the National Technical Information Service.

If your address has changed, or if you wish to be removed from the mailing list, or if the addressee is no longer employed by your organization, please notify PL/TSI, 29 Randolph Road, Hanscom AFB, MA 01731-3010. This will assist us in maintaining a current mailing list.

Do not return copies of this report unless contractual obligations or notices on a specific document requires that it be returned.

REPORT DOCUMENTATION PAGE

Form Approved
OMB No. 0704-0188

Public reporting burden for this collection of information is estimated to average 1 hour per response, including the time for reviewing instructions, searching existing data sources, gathering and maintaining the data needed, and completing and reviewing the collection of information. Send comments regarding this burden estimate or any other aspect of this collection of information, including suggestions for reducing this burden, to Washington Headquarters Services, Directorate for information Operations and Reports, 1215 Jefferson Davis Highway, Suite 1204, Arlington, VA 22202-4302, and to the Office of Management and Budget, Paperwork Reduction Project (0704-0188), Washington, DC 20503

1. AGENCY USE ONLY (Leave blank)	2. REPORT DATE	3. REPORT TYPE AND DATES COVERED
	14 MAY 1994	Scientific No. 1

4. TITLE AND SUBTITLE
SEISMIC STUDIES OF THE CASPIAN BASIN AND SURROUNDING REGIONS

5. FUNDING NUMBERS
PE 61102F
PR 2309 TA G2 WU BM
Contract F49620-92-J-0475

6. AUTHOR(S)
STEPHEN MANGINO
KEITH PRIESTLEY

7. PERFORMING ORGANIZATION NAME(S) AND ADDRESS(ES)
University of Cambridge
Dept of Earth Sciences
Madingley Rise, Madingley Road
Cambridge CB3 OEZ, UK

8. PERFORMING ORGANIZATION REPORT NUMBER

9. SPONSORING/MONITORING AGENCY NAME(S) AND ADDRESS(ES)
Phillips Laboratory
29 Randolph Road
Hanscom AFB, MA 01731-3010

Contract Manager: James Lewkowicz/GPEH

10. SPONSORING/MONITORING AGENCY REPORT NUMBER
PL-TR-94-2152

11. SUPPLEMENTARY NOTES

12a. DISTRIBUTION/AVAILABILITY STATEMENT
APPROVED FOR PUBLIC RELEASE DISTRIBUTION UNLIMITED

12b. DISTRIBUTION CODE

13. ABSTRACT (Maximum 200 words)

In order to investigate the anomalous crust and upper mantle structure of the south Caspian Basin, we installed a network of six three-component seismograph stations within the former Soviet republics of Turkmenistan and Azerbaijan. Our objective is to determine the velocity structure of this region using both body wave receiver function and surface wave modeling techniques. This first year report documents the seismograph network installation and data processing methods, discusses the crustal velocity structure for one network station in Turkmenistan and describes surface wave observations for paths across the south Caspian Basin.

14. SUBJECT TERMS
Crustal Structure, Upper Mantle Structure, Surface Waves, Receiver Function Inversion, Caspian Basin.

15. NUMBER OF PAGES
34

16. PRICE CODE

17. SECURITY CLASSIFICATION OF REPORT	18. SECURITY CLASSIFICATION OF THIS PAGE	19. SECURITY CLASSIFICATION OF ABSTRACT	20. LIMITATION OF ABSTRACT
Unclassified	Unclassified	Unclassified	SAR

Table of Contents

Accesion For

NTIS CRA&I ☒

DTIC TAB ☐

Unannounced ☐

Justification .....

By .....

Distribution /

Availability Codes

Dist	Avail and / or Special
A-1	

1. Introduction

This report documents our research efforts during the first year of USAF grant F49620-92-J-0475. The objective of these efforts is two fold: first, to characterize the crust and upper mantle velocity structure of the south Caspian Basin using both body-wave receiver function and surface wave dispersion techniques, and second, to understand the structural effects on regional seismic wave propagation. To accomplish this, a network of 6 digital three-component seismic stations has been installed in the former Soviet republics of Turkmenistan and Azerbaijan. Section 2 describes the regional tectonic setting of the south Caspian Basin. Section 3 documents the seismograph network installation, calibration and data processing methods. Section 4 discusses the crustal receiver response and the preliminary modeling results of one station in the western Turkmenian Lowlands. Section 5 describes surface wave observations for paths across the southern Caspian Basin.

2. Tectonic Setting

The south Caspian Basin is an anomalous aseismic depression that is surrounded by active fold and thrust belts that are part of the east-west trending Alpine-Himalayan Belt. The Basin is bounded to the north by a narrow seismogenic zone extending from the Caucasus Mountains in Azerbaijan, through the Apsheron-Balkhan Sill, to the Kopet Dag Mountains of Turkmenistan. To the west in Azerbaijan and to the south along the Iranian border the Basin is bounded by the active fold and thrust belts of the Talesh and Alborz Mountains, respectively. Located to the east of the Caspian Sea are the Turkmenian Lowlands which are structurally a part of the south Caspian Basin. Within the Basin near Baku there is evidence of shallow volcanic activity (Glibkin, 1971).

Deep seismic sounding (DSS) data collected in the early 1960's suggests that the crust of the south Caspian Basin and west Turkmenian Lowlands consists of 2 layers; a thick sedimentary layer (15-20 km) with a P-wave velocity of 3.5-4.0 km/s which overlies a 12-18 km thick 'basaltic' layer with a P-wave velocity of 6.6-7.0 km/s (Neprochnov 1968;

Rezanov and Chamo, 1969). It has been suggested that the south Caspian Basin represents a section of 'ocean-like crust' that may be either a relic of an older Paleozoic-Triassic ocean, or alternatively a marginal sea which developed behind a Mesozoic-Paleogene ocean (Berberian and King 1981; Berberian 1983). The 'ocean like' crust hypothesis is supported by the observation of L_g blockage and efficient S_n propagation for the paths that cross the south Caspian Basin (Kadinsky-Cade et al., 1981). The northward movement of the Iranian plate with respect to the Eurasian plate is causing compressional deformation throughout this region (Jackson and McKenzie 1984). A focal mechanism analysis of earthquakes that occurred within the seismic belts bordering the Basin suggest that the crustal shortening between Iran and Eurasia is being accommodated primarily along thrust and strike-slip faults in the Alborz and Talesh Mountains, and to a lesser extent, by northern Caspian continental crust thrust over the south Caspian Basin 'ocean-like' crust (Priestley et al., 1994).

3. The South Caspian Basin Seismograph Network (CSN)

During May, June, and December 1993 a network of 6 three-component seismograph stations was installed in the former Soviet republics of Turkmenistan and Azerbaijan. The Turkmenian stations are located near Krasnovosdk (KRV), Nebit Dag (NBD), Dana Tag (DTA) and Kizyl Atrek (KAT) (Figure 1). In Azerbaijan the stations are located near Lenkoran (LNK) and Baku (BAK) (Figure 1). The installation and ongoing station maintenance are made possible by the logistical support of Dr. M. Roshkov and Dr. V. Kiseleivich, both of whom are from the Institute for Research in Seismology (IRIS) Moscow Data Center. The Turkmenian stations are located at previously existing seismograph stations and are operated in cooperation with Dr. B. Karryev from the Institute of Seismology of Turkmenistan. The two Azerbaijan stations are also located at previously established seismograph stations and are operated in cooperation with Dr. S. Agamirzoev from the Geophysical Expedition of Azerbaijan. The technical support and software available at the IRIS Equipment Center located at Lamont Doherety Geological Observatory

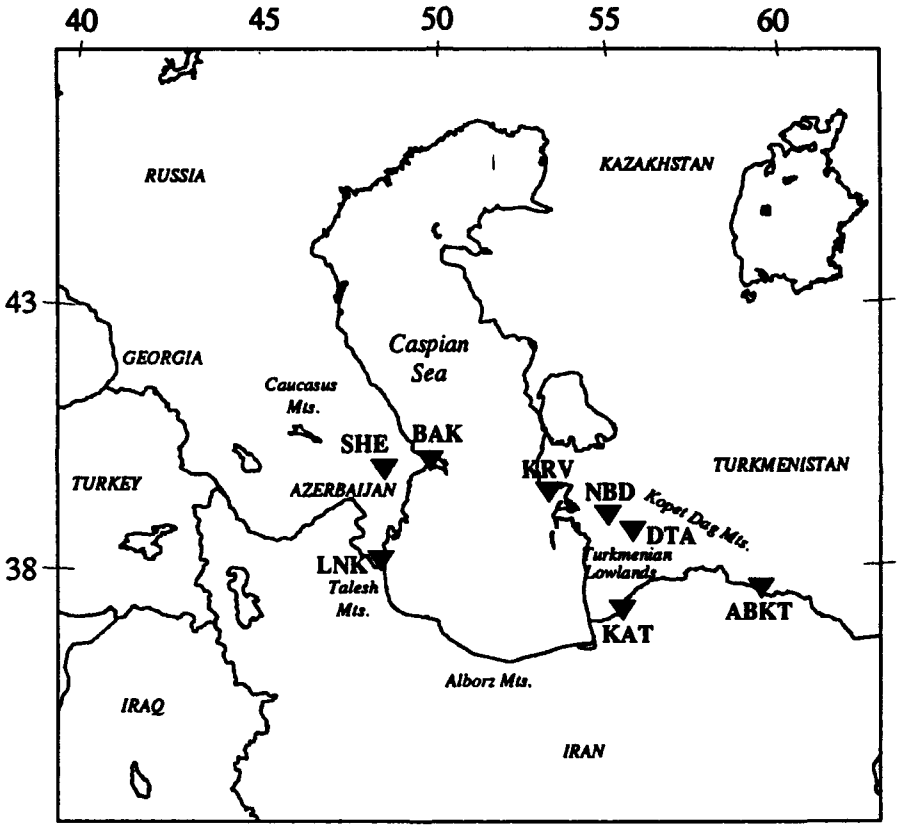

Figure 1. Map of the Caspian Sea and surrounding region.

are equally indispensable. In addition to the data from our seismograph network, this study incorporates data from the IRIS seismograph station near Ashkabat, Turkmenistan (ABKT) (Figure 1).

3.1 Instrumentation

Data at each CSN station is recorded on a Refraction Technology 72a-02 data logger which is equipped with either Omega or GPS timing and an external hard disk. Four stations (KRV, DTA, KAT and LNK) record ground motion using a Guralp CMG-3T triaxial broadband (BB) feedback seismometer. Two stations (NBD and BAK) have three component Teledyne Geotech SL-210/220 long period (15 second free period) (LP) pendulum seismometers. All six stations record data continuously. Data is transferred from disk to magnetic tape once every two months. The only significant problems that have been encountered thus far are seismometer drift and local power outages. To correct for drift we designed and installed a clock based re-centering unit at each BB station. This device issues a 'center' command to the CMG-3T at weekly intervals. Additionally, the LP stations are periodically manually re-centered.

3.2 Station Installation

Station KRV (40.006N 52.957E -7m) was installed in May, near the city of Krasnovosdk. The station is located about 3 km east of the Caspian Sea along the western edge of the Krasnovosdk Plateau. Topography in the vicinity of the station is moderate with elevation changes up to 100 meters. The seismometer is installed on a decoupled cement pier within a concrete vault 8 meters beneath the surface. This pier overlies bedrock.

Station NBD (39.507N 54.387E -18m) was installed in May, in the semi-arid town of Nebit Dag. The station is approximately 80 km east of the Caspian Sea within the western Turkmenian Lowlands. Topography throughout the Lowlands is relatively flat with elevation changes of less than 10 meters. The seismometer is installed on a cement pier within a vault

8m beneath the surface. The pier is not de-coupled from the building and overlies unconsolidated sediments i.e. sand and clay. Station NBD was initially installed with a BB seismometer. In October, we replaced the BB seismometer with three LP seismometers.

Station DTA (39.075N 55.165E +319m) was installed in December, near the village of Dana Tag. The station is in the foothills of the Kopet Dag Mountains just east of the Lowlands. The seismometer is installed in a surface vault on a decoupled cement pier. The pier overlies weathered shale, silt stone and gravel. In June 1994 we plan to initiate a second event triggered data stream at 50 sps.

Station KAT (37.669N 54.776E +84m) was installed in May, near the village of Kizyl-Atrek. The station is 1 km north of the Iranian border and is about 20 km north of the Alborz Mountain front. Topography in the vicinity of the station is minimal. The seismometer is installed on a cement pier within a vault 5 meters beneath the surface. The pier is not decoupled from the building and overlies alluvium.

Station LNK (38.710N 48.779E -2m) was installed in June, near the city of Lenkoran. The station is approximately 8 km southwest of Lenkoran and is about 10 km west of the Caspian Sea. Topography in the vicinity of the station is moderate with elevation changes up to 100m. The seismometer is installed on a decoupled cement pier within a surface vault that overlies bedrock. A small industrial complex 3 km east of the station is a minor source of noise.

Station BAK (40.581N 49.987E -27m) was installed in June, about 40 km north of Baku the capital of Azerbaijan. The station is on the Apsheron Peninsula and is about 1 km from the Caspian Sea. Topography in the vicinity of the station is minimal. The seismometers are installed on a decoupled cement pier within a surface vault. The pier overlies unconsolidated sands and sandstone. We plan to relocate BAK to station SHE (Figure 1) in June 1994 because the BAK site has been found to be unstable for long period recording.

3.3 Calibration

To determine the instrument transfer function each station is calibrated with a step function and with a pseudo-random binary input. Figure 2 shows the step calibration response normalized to a common network sensitivity, for all channels at each station. For long periods a step function is sufficient to characterize the instrument response. This is because the power spectral density of a step function decreases as $1/\omega^2$ and therefore, most of the power is limited to long periods. The pseudo-random binary input (RB) consists of a series of fixed amplitude step functions which vary randomly in duration. The RB signal has a nearly flat power spectral density of up to half the frequency of the RB clock rate (Berger et al., 1979). We designed one RB calibrator and three step calibrators for the CSN. This was done in order to determine the instrument response to an accuracy of 1 percent in amplitude and 1° in phase. Step calibrations have been routinely performed since station installation and the RB calibrations will be performed in June 1994.

3.4 Data Processing

Data processing and data archival can be briefly broken down into three basic components. First, all CSN station raw data files are permanently archived to tape. The amount of data, depending on station 'uptime' can exceed 2 Giga bytes for every two months of continuous recording. Second, the data is converted into SEGY format and plotted per Julian day. Individual events are identified with respect to the Preliminary Determination of Epicenter (PDE) and Quick Epicentral Determination (QED) Bulletins and then merged into continuous event record files. Third, the data is converted into SAC format (Tapley and Tull, 1991) and event file headers are updated with the appropriate source and station information. Figure 3 shows the first minute of a teleseismic event recorded at the Turkmenian Lowland station NBD. This event is typical of those teleseismic events discussed in the receiver function section of this report. A number of local and regional events have also been recorded that are not identified in either the PDE or QED. Listed in

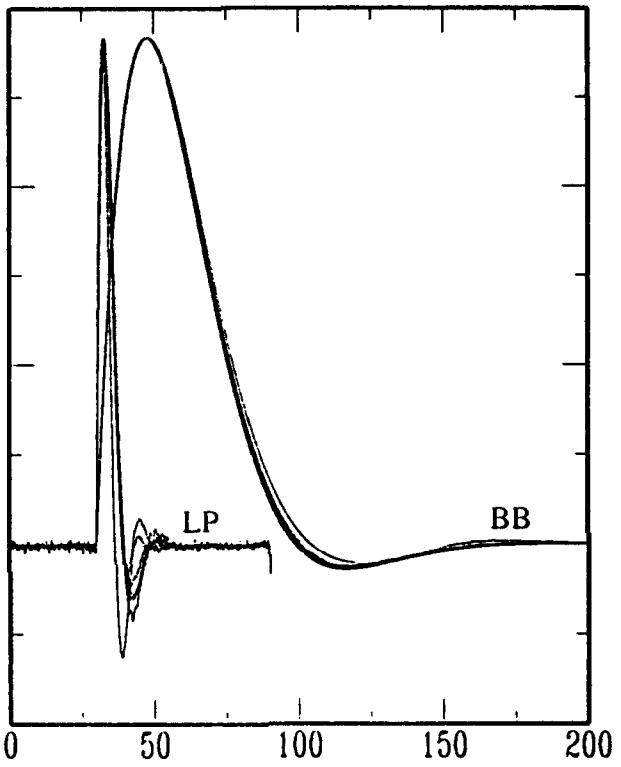

Figure 2. The response due to an input step in voltage for all Guralp CMG-3T broadband (BB) channels and all Teledyne Geotech SL-210/220 long period (LP) channels normalized to a common network sensivitity.

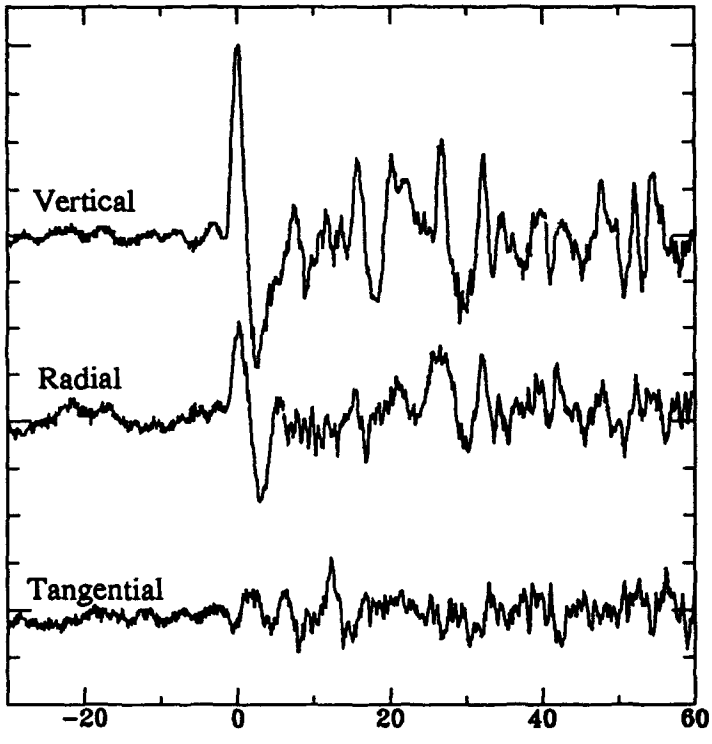

Figure 3. First minute of a typical teleseism recorded at CSN station NBD, with a backazimuth of 41.3 and an epicentral distance of 67.6 degrees.

Table 1 are all events processed from onset of the experiment through December 1993. In reference to Table 1, the right hand column indicates if the event was recorded at that station (1=yes, 0=no). The numbering of each station is as follows: KRV=1; NBD=2; KAT=3; LNK=4; and BAK=5.

4. Receiver Function Analysis

In the first 30 seconds following the direct P-wave, multiply reflected and converted phases are generated by the interaction of the incoming direct P-wave and the receiver structure beneath the recording station. The source equalization method of (Langston 1979; Ammon 1991) is used to isolate the converted shear phases (P-SV) which are primarily recorded on the horizontal components of ground motion. The resulting source equalized radial and tangential component time series are called receiver functions. Receiver functions obtained from events with a common azimuth and epicentral distance are stacked to improve the signal to noise ratio. The variance of the stacked data represents a measure of coherence of individual phases. Individual or stacked radial component receiver functions are then used to estimate the receiver structure with models composed of either vertically heterogeneous and laterally homogeneous horizontal layers, or two-dimensional models composed of planer dipping layers. For a one-dimensional model the radial receiver function is composed of P-SV energy that propagates within the vertical plane between the source and receiver while the tangential receiver function is zero.

For a plane P-wave incident at the base of a dipping layer, P-SV energy is coupled with SH, therefore, the tangential component is non-zero. Two key indicators of a planer dipping structure beneath a recording station are: (1) a systematic polarity variation of scattered energy on the tangential response as a function of azimuth; and (2), a moveout with respect to the direct P-wave, of multiply reflected and converted phases as a function of the incident P-wave azimuth to the dipping layer (Langston 1977). Observations of these effects at other

seismograph stations are discussed in Owens and Crosson (1988) and in Mangino and Ebel (1991).

In receiver function modeling a primary concern is the contamination of the radial receiver function with scattered energy. Contamination can be estimated by analysis of the tangential receiver function. By varying the width of the Gaussian filter in the source equalization procedure, all, or part of the bandwidth available can be examined. In some cases, lower frequency receiver functions are simpler than their higher frequency counterparts and are potentially less-biased by small scale (relative to wavelength) lateral heterogeneity.

4.1 The Response at CSN station NBD

Figure 4 shows the NBD radial and tangential (0.01-0.5 Hz) receiver functions as a function of backazimuth. The large amplitude arrivals present on the NBD radial response indicate the receiver structure beneath NBD contains prominent velocity contrasts. In comparison with the radial, motion on the tangential is low for the north-easterly backazimuths. This is consistent with, but not necessarily limited to, the response of one-dimensional model. The difference between the radial and tangential response as a function of azimuth suggests some lateral heterogeneity. As backazimuth increases to more easterly approaches, motion on the tangential component between 12-14 seconds increases and eventually exceeds the amplitude of the radial response. As more data is collected a complete picture may emerge for station NBD. For the present analysis, the 41° backazimuth two event stack is examined in detail below.

The DSS modeling results given in Rezanov and Chamo (1969) are used for preliminary comparison to the NBD response. Figure 5 shows the Rezanov and Chamo (1969) velocity model for the western Turkmenian Lowlands and the corresponding synthetic receiver function determined from this model compared to the NBD data. Agreement is poor between the DSS model synthetic receiver function and the NBD data.

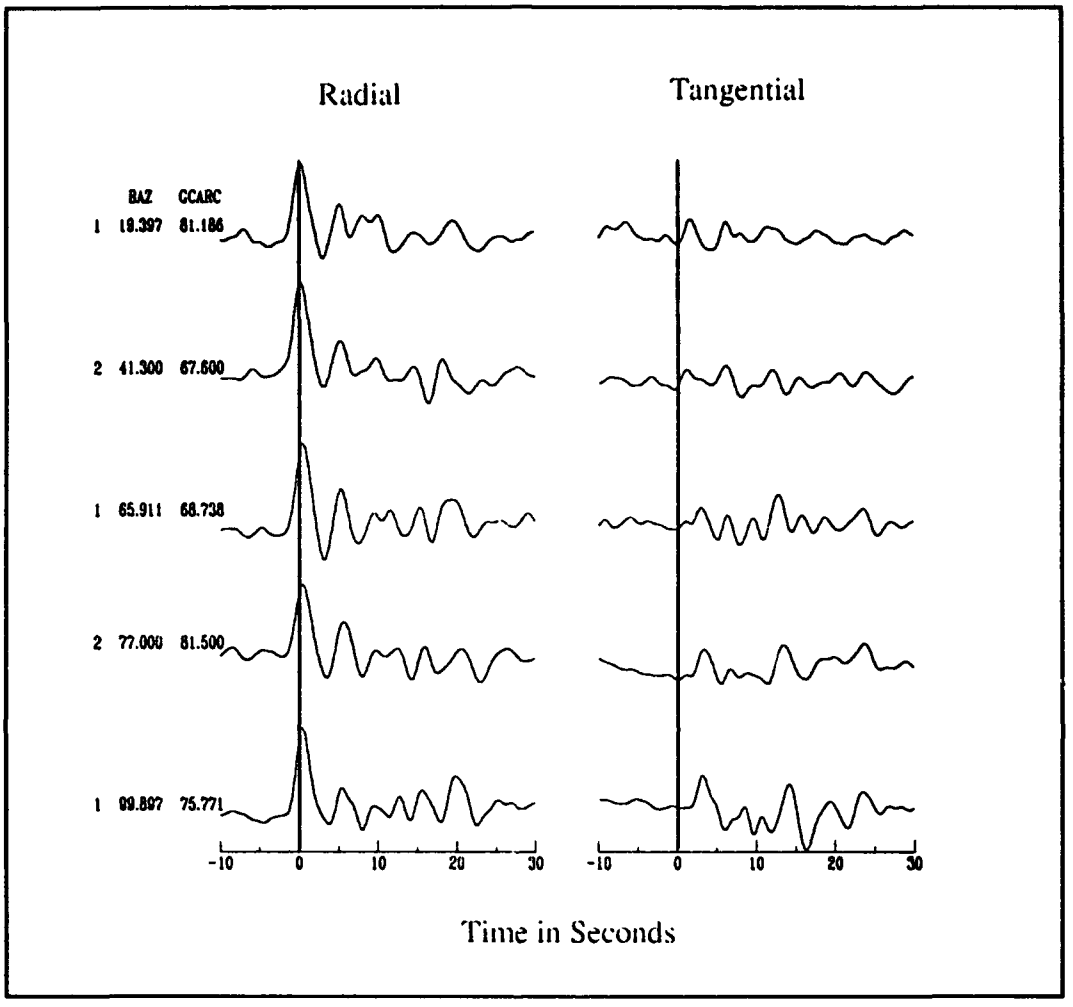

Figure 4. Station NBD Radial (left) and Tangential (right) receiver functions clockwise from north about the station, relative amplitudes are preserved. The number of events stacked, epicentral distance and backazimuth is indicated to the left of each trace pair.

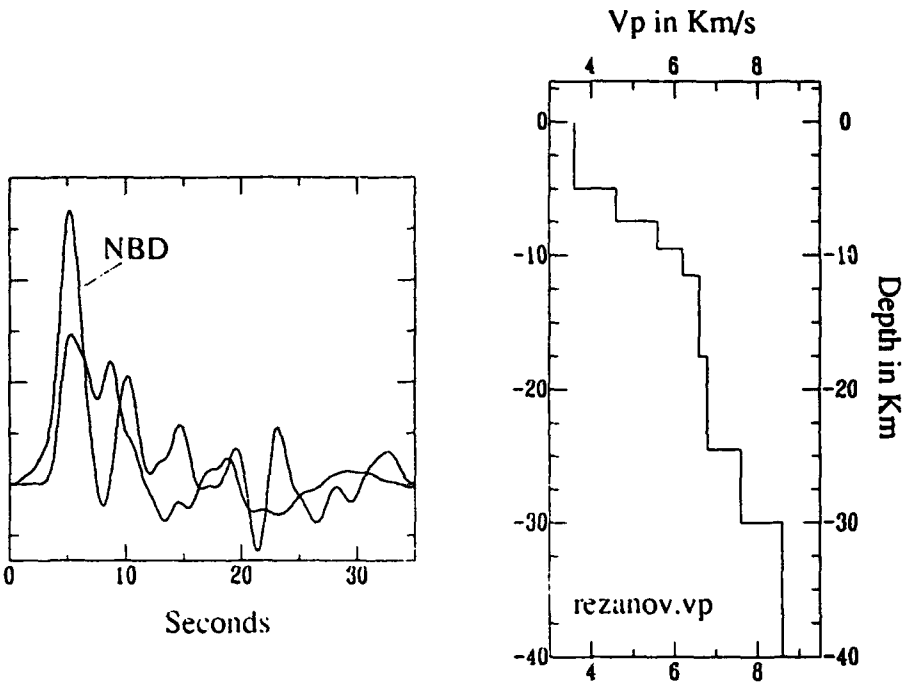

Figure 5. Comparison between the DSS results of Rezanov and Chamo (1969) for the Turkmenian Lowlands (right) and model synthetic receiver function (left) with the NBD stacked data.

To determine the crustal structure beneath station NBD the time domain inversion procedure of Ammon et al. (1990) is employed. The NBD stacked data is linearized in a Taylor series about the starting model, obtained from forward modeling. Each model layer is perturbed and a waveform derivative is determined for each perturbation. The L_2 norm between the model synthetic receiver function and the observed data, with a side constraint of model smoothness, is then minimized. A Poisson's ratio of 0.25 is used to relate P- to S-wave velocity. The resulting solution model synthetics that do not fit the most coherent phases in the data are discarded, and the remaining solution models represent the crustal structure beneath the station. It is important to recognize at this point a limitation of this technique's inability to constrain absolute depth-to-interface velocity. Herein lies the importance of apriori information which can be used to select a model or 'family' of models if a range solution models exist.

4.2 NBD Modeling Results

Figure 6 shows the inversion results for the NBD 2 event stack. The most important model features are a strong positive gradient from the surface to 4 km depth, a 3-4 km thick high velocity layer, and a prominent decrease in velocity between 8-9 km depth. Between 10 to 20 km depth, the 'mid-crust' average velocity is between 5.8-6.2 km/s. At a depth of 20-24 km, velocity increases to 6.8-7.2 km/s, and has a positive gradient through the 'lower crust' to a depth of 34 km, where velocity jumps by 0.5 km/s to 8.0-8.1 km/s.

The most prominent and suspect model feature is the 4 km thick high velocity layer in the upper crust. This 'layer' is the most significant contributor to the large amplitude arrivals in the first 10 seconds of data. The broad direct arrival is matched with Ps conversions from the top of the positive gradient in layers 1-4. The large negative motion between 2-3 seconds are fit with reverse polarity Ps conversions from the base of the shallow high velocity layer. First order multiples from the top and bottom of this 'layer' also contribute to the response. Direct comparison of the radial and tangential response (Figure

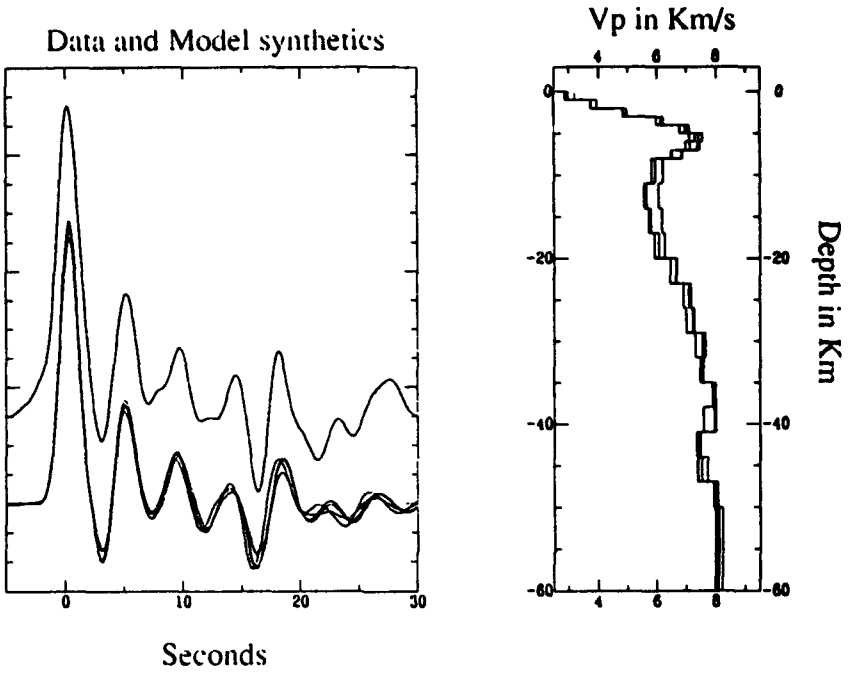

Figure 6. Inversion results for station NBD (right) and the model synthetic receiver functions (lower left) compared to the stacked data (upper left).

5) indicate the shear wave energy is predominately confined within the vertical plane. Therefore, it is difficult to attribute this model feature to an artifact of scattering. Speculation on the significance of this 'layer' within a relatively simple crustal structure is premature until more data is recorded at station NBD, and the adjacent stations KRV and DTA are modeled in detail.

5. Surface Wave Observations

Figure 7 shows vertical component seismograms from a mid-Atlantic ridge earthquake that were recorded at stations LNK and KRV. These stations lie on almost the same great circle path from the epicenter and both stations have identical instrumentation. Previous analysis of short-period seismograms has shown that the higher frequency (0.5-2.0 Hz) crustal phase L_g is not observed for paths that cross the south Caspian Basin (Kadinsky-Cade et al., 1981). Figure 7 shows that both the shorter period and longer period surface wave train is strongly attenuated or scattered across the south Caspian Basin.

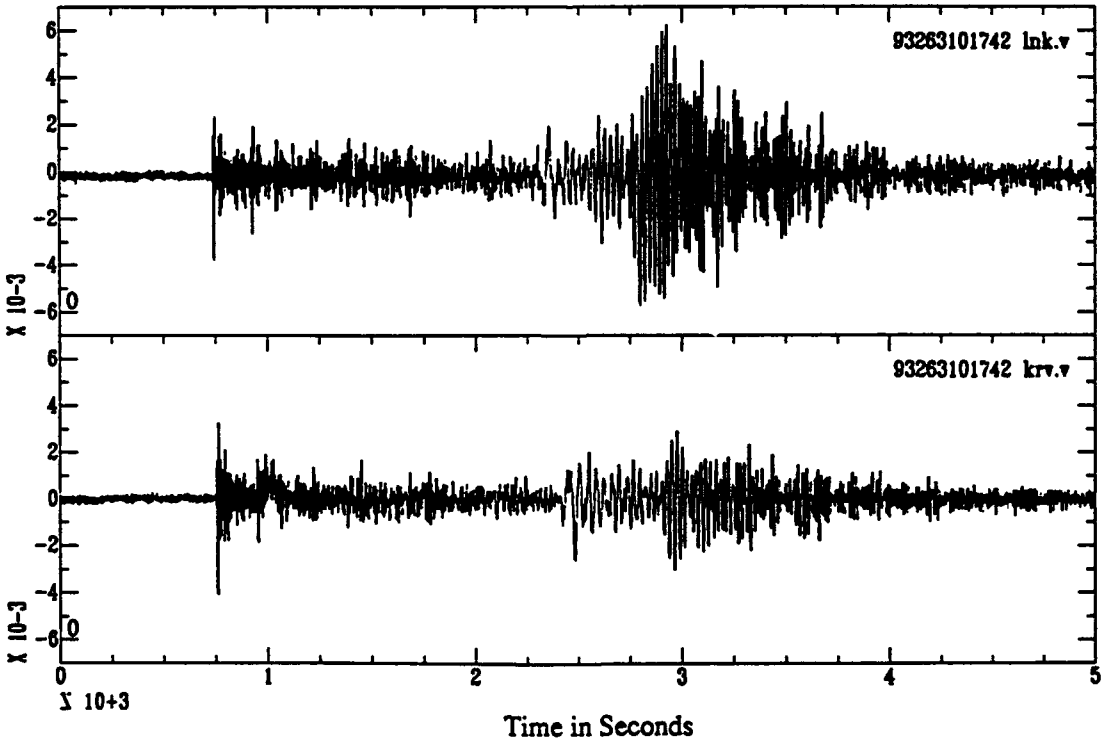

Figure 7. Vertical component seismograms from a Mid-Atlantic Ridge earthquake (Ms=5.9) recorded at station LNK (top) and KRV (bottom).

Table 1

1993 Caspian Network Data: Julian Days 143->344

Date	Origin Time (UTC)	Lat	Lon	Z	Mb	Ms	Event Location	sta 12345
143 MAY 23	161831	46.535	153.218	33	5.0		KURIL ISLANDS	01100
144 MAY 24	235121	-23.612	-66.869	239	6.2		JUJUY PROVINCE, ARGENTINA.	11100
145 MAY 25	231643	55.086	-160.421	33	6.2	5.8	ALASKA PENINSULA.	11100
148 MAY 28	155527	55.880	-155.199	33	5.0	4.9	SOUTH OF ALASKA	11100
149 MAY 29	065013	19.104	-26.499	10	5.8	6.1	NORTH ATLANTIC OCEAN	11100
150 MAY 30	170851	1.549	127.180	56	5.9	5.2	HALMAHERA, INDONESIA	11110
150 MAY 30	223359	-0.578	124.184	33	5.6	5.2	SOUTHERN MOLUCCA SEA	11110
151 MAY 31	083421	-72.455	174.681	10	4.9	5.1	ROSS SEA	11110
152 JUN 1	094530	34.661	26.548	33	5.0		CRETE	11100
152 JUN 1	155347	-45.650	-77.110	33	5.1	5.4	OFF COAST OF SOUTHERN CHILE	11100
153 JUN 2	030016	-46.276	33.428	10	5.2	5.6	PRINCE EDWARD ISL	11100
153 JUN 2	082720	51.523	-178.727	48	5.6	5.4	ANDREANOF ISL ALEUTIANS	11100
154 JUN 3	201624	9.538	126.601	33	5.0	4.9	MINDANAO, PHILIPPINE ISLANDS	11100
155 JUN 4	030637	11.908	142.446	39	5.5	5.4	SOUTH OF MARIANA ISLANDS	11100
155 JUN 4	104937	3.840	128.373	53	5.8	5.8	NORTH OF HALMAHERA, INDONESIA.	11100
157 JUN 6	132324	15.893	146.526	33	5.9	6.6	MARIANA ISLANDS.	11100
158 JUN 7	074935	36.006	141.579	33	5.4	5.2	NEAR EAST COAST OF HONSHU, JAPAN	11100
158 JUN 7	131442	35.299	141.677	44	5.2	4.8	NEAR EAST COAST OF HONSHU, JAPAN	11100
159 JUN 8	130334	51.243	157.806	51	6.5	7.2	NEAR EAST COAST OF KAMCHATKA.	11100
159 JUN 8	231741	-31.452	-68.987	113	6.4		SAN JUAN PROVINCE, ARGENTINA.	11100
160 JUN 9	173336	34.786	53.246	33	4.8		NORTHERN IRAN	11100
161 JUN 10	120457	50.929	159.521	33	5.5	5.0	EAST OF KURIL ISLANDS	11100
163 JUN 12	054524	-11.082	162.937	33	5.4	6.0	SOLOMON ISLANDS	11100
163 JUN 12	182645	-4.432	135.071	33	5.9	6.2	IRIAN JAYA REGION, INDONESIA.	11100
163 JUN 12	203326	51.256	157.744	49	6.0	5.8	NEAR EAST COAST OF KAMCHATKA.	11100
164 JUN 13	232640	39.339	20.621	20	5.2		GREECE-ALBANIA BORDER REGION	11100
165 JUN 14	073018	35.710	78.459	33	5.0	4.5	EASTERN KASHMIR	11100
165 JUN 14	195942	39.374	38.203	33	4.9		TURKEY.	11100
166 JUN 15	044256	34.857	141.715	42	5.1	5.2	OFF EAST COAST OF HONSHU, JAPAN	11100
166 JUN 15	231226	35.718	77.560	33	4.9		EASTERN KASHMIR	11100
168 JUN 17	204446	36.507	71.337	33	5.2		AFGHANISTAN-TAJIKISTAN BORD REG.	11000
169 JUN 18	115251	-29.392	-176.742	21	6.2	6.6	KERMADEC ISL	11000
169 JUN 18	175748	-28.537	-176.848	20	5.9	6.7	KERMADEC ISL	11000
170 JUN 19	122330	10.174	-103.647	10	5.2	5.3	OFF MEXICO	11000
170 JUN 19	170156	36.551	54.860	33	4.5		NORTHERN IRAN	11000
171 JUN 20	020925	-6.269	130.165	157	5.3		BANDA SEA	11000
171 JUN 20	172638	-7.045	155.693	105	5.3		SOLOMON ISLANDS	11000
173 JUN 22	123347	64.729	-17.340	10	5.2	4.8	ICELAND	11000
173 JUN 22	163244	30.254	50.855	33	5.6	4.8	NORTHERN IRAN.	11000
174 JUN 23	112918	-60.630	-56.460	10	5.7	5.3	SOUTH SHETLAND ISLANDS	11000
175 JUN 24	001519	20.054	121.459	33	5.1	4.7	PHILIPPINE ISLANDS REGION	11000
186 JUL 5	005241	-24.891	-112.554	10	5.3	5.5	EASTER ISLAND REGION.	00010
186 JUL 5	065409	8.543	-102.887	10	4.9	5.1	OFF COAST OF MEXICO	00010
187 JUL 6	025302	-24.709	-112.019	10	5.5	6.0	EASTER ISLAND REGION.	00010
188 JUL 7	111053	27.807	128.058	43	5.0	4.9	RYUKYU ISLANDS	10010
188 JUL 7	204910	51.102	159.532	33	5.2	4.6	OFF EAST COAST OF KAMCHATKA	10010
189 JUL 8	182218	-20.713	172.244	33	5.5	6.0	VANUATU ISLANDS REGION.	10110
189 JUL 8	104625	51.154	159.249	33	5.2	5.1	OFF EAST COAST OF KAMCHATKA	10010
190 JUL 9	102923	28.415	55.190	33	5.2	4.6	SOUTHERN IRAN	10110
190 JUL 9	153755	-29.683	-177.604	412	5.8		FIJI ISLANDS REGION.	10110

Table 1 (continued)

Date	Origin Time(UTC)	Lat	Lon	Z	Mb	Ms	Event Location	sta 12345
192 JUL 11	133619	-25.351	-70.177	33	6.2	6.0	NORTHERN CHILE	10100
192 JUL 11	174809	47.590	154.182	21	5.7	5.3	KURIL ISL	10100
193 JUL 12	050531	72.178	1.097	10	5.1	4.9	NORWEGIAN SEA	10100
193 JUL 12	131711	42.841	139.248	17	6.7	7.6	HOKKAIDO	10100
194 JUL 13	083555	-3.228	145.591	33	5.1	5.7	NEAR N COAST OF NEW GUINEA, PNG.	10100
194 JUL 13	142254	37.400	55.550	33	4.6		TURKMENISTAN-IRAN BDR	10100
195 JUL 14	123151	38.401	21.721	33	5.2	5.4	GREECE.	10100
195 JUL 14	173836	43.184	139.233	33	5.5	4.5	EASTERN SEA OF JAPAN	10100
196 JUL 15	005113	46.671	152.580	33	5.7	4.7	KURIL ISLANDS	10100
196 JUL 15	193739	42.657	139.008	33	5.3	4.4	HOKKAIDO, JAPAN REGION.	10100
198 JUL 17	094635	28.001	99.691	33	5.4	4.7	YUNNAN, CHINA.	10100
200 JUL 19	191840	43.098	139.126	33	5.0	4.6	EASTERN SEA OF JAPAN	10100
202 JUL 21	220633	13.360	-90.874	33	5.0	5.2	NEAR COAST OF GUATEMALA	10100
203 JUL 22	045707	6.498	-71.226	19	6.0	5.9	NORTHERN COLOMBIA.	10100
203 JUL 22	121536	21.796	144.229	127	5.5		MARIANA ISLANDS REGION.	10100
204 JUL 23	115008	36.418	70.442	287	5.1		HINDU KUSH REGION, AFGHANISTAN.	10100
205 JUL 24	020200	5.071	127.678	150	5.5		PHILIPPINE ISLANDS REGION	10100
205 JUL 24	102656	51.518	-176.854	33	5.1	4.2	ANDREANOF ISLANDS, ALEUTIAN IS.	10100
207 JUL 26	100419	2.983	125.735	100	5.0		TALAUD ISL, INDONESIA	10100
208 JUL 27	194450	34.447	141.628	33	5.1	4.8	OFF EAST COAST OF HONSHU, JAPAN	00100
209 JUL 28	171640	46.411	150.895	86	5.2		KURIL ISLANDS	00100
209 JUL 28	180749	-5.588	154.103	33	5.4	6.0	SOLOMON ISLANDS	00100
211 JUL 30	233408	28.606	34.657	10	4.8		EGYPT	00100
212 JUL 31	231320	56.105	112.484	33	4.7		LAKE BAYKAL REGION, RUSSIA	00100
213 AUG 1	002040	15.581	31.918	10	5.2	5.2	SUDAN.	00100
213 AUG 1	193229	17.419	-65.695	33	5.0	4.4	PUERTO RICO REGION.	00100
214 AUG 2	031321	30.844	131.447	33	5.5	5.2	KYUSHU, JAPAN	00100
214 AUG 2	164818	36.993	71.388	150	4.6		AFGHANISTAN-TAJIKISTAN BORD REG.	00100
215 AUG 3	072000	51.382	-130.521	10	5.5	5.9	QUEEN CHARLOTTE ISLANDS REGION.	00100
215 AUG 3	124304	28.634	34.719	10	6.1	5.7	EGYPT.	00110
215 AUG 3	125405	28.200	34.570	10	5.2		EGYPT	00110
215 AUG 3	163320	28.650	34.726	10	5.7	5.1	EGYPT.	00110
216 AUG 4	113118	-1.604	99.689	33	6.1	6.4	SOUTHERN SUMATERA, INDONESIA.	00110
217 AUG 5	070533	72.369	1.809	10	4.7	4.5	NORWEGIAN SEA	00110
217 AUG 5	230511	3.717	127.526	33	4.8	3.9	TALAUD ISLANDS, INDONESIA	00110
219 AUG 7	000037	26.528	125.612	158	6.0		NORTHEAST OF TAIWAN.	00110
219 AUG 7	175327	-23.904	179.793	560	6.0		SOUTH OF FIJI ISLANDS.	00010
219 AUG 7	194244	41.950	139.863	33	6.1	5.9	HOKKAIDO, JAPAN REGION.	00010
220 AUG 8	200315	13.469	145.604	60	5.3	5.8	MARIANA ISLANDS.	00110
220 AUG 8	224145	38.677	70.647	33	5.0	4.7	AFGHANISTAN-TAJIKISTAN BORD REG.	00110
220 AUG 8	003109	0.855	120.403	62	5.4	4.9	MINAHASSA PENINSULA, SULAWESI	00010
220 AUG 8	083425	12.971	144.744	61	7.0	8.0	SOUTH OF MARIANA ISLANDS.	00010
221 AUG 9	060502	28.613	34.762	10	4.9		Egypt	00110
221 AUG 9	091516	13.415	145.610	60	5.3	5.5	MARIANA ISLANDS	00110
221 AUG 9	113833	36.395	70.707	230	5.8		HINDU KUSH REGION, AFGHANISTAN	00110
221 AUG 9	124250	36.348	70.840	233	6.3		HINDU KUSH REGION, AFGHANISTAN.	01100
222 AUG 10	005154	-45.205	166.929	33		7.1	OFF W. COAST OF S. ISLAND, N.Z.	11100
222 AUG 10	055821	40.154	22.991	10	4.6		GREECE	11100
222 AUG 10	094639	-38.418	177.439	33	5.8	6.0	NORTH ISLAND, NEW ZEALAND.	11100

Table 1 (continued)

Date	Origin Time(UTC)	Lat	Lon	Z	Mb	Ms	Event Location	sta 12345
222 AUG 10	193621	82.993	-28.130	10	5.4	4.9	NEAR NORTH COAST OF GREENLAND	11100
223 AUG 11	141742	13.122	145.626	60	5.9	6.2	MARIANA ISLANDS.	11100
224 AUG 12	094811	48.264	154.641	35	4.7		KURIL ISLS	11100
225 AUG 13	110221	-35.971	178.496	108	5.7		OFF E. COAST OF N. ISLAND, N.Z.	11100
226 AUG 14	035239	37.660	70.950	33	4.8		AFGHANISTAN-TAJIKISTAN BORD REG.	11100
226 AUG 14	143003	25.422	101.373	33	4.8	4.7	YUNNAN, CHINA	11100
227 AUG 15	031021	0.923	-25.866	15	5.3	5.3	CENTRAL MID-ATLANTIC RIDGE	11100
228 AUG 16	043350	12.988	144.949	33	5.7	6.0	SOUTH OF MARIANA ISLANDS.	11100
231 AUG 19	080323	13.251	145.452	60	5.5		MARIANA ISLANDS.	11000
231 AUG 19	152142	7.168	126.808	70	5.4		MINDANAO, PHILIPPINE ISLANDS	11000
231 AUG 19	215205	7.150	126.796	33	5.2	4.4	MINDANAO, PHILIPPINE ISLANDS	11000
232 AUG 20	050652	-6.025	142.699	10	5.9	6.2	NEW GUINEA, PAPUA NEW GUINEA.	11000
235 AUG 23	052144	29.955	67.888	33	4.9		PAKISTAN	11000
236 AUG 24	174731	20.737	71.494	33	5.0		SOUTHERN INDIA.	11000
237 AUG 25	052531	-44.875	-79.944	10	5.4	5.4	OFF COAST OF SOUTHERN CHILE.	11000
238 AUG 26	013000	-35.906	178.301	33	5.4	5.4	OFF E. COAST OF N. ISLAND, N.Z.	11000
238 AUG 26	100356	36.738	28.193	33	5.2		DODECANESE ISLANDS	11000
238 AUG 26	213233	45.699	26.634	143	5.1		ROMANIA.	11000
240 AUG 28	201444	6.515	94.704	121	5.8		NICOBAR ISLANDS, INDIA	11000
241 AUG 29	095755	-6.998	129.577	150	5.6		BANDA SEA	11000
243 AUG 31	065531	41.855	49.523	70	5.5		CASPIAN SEA.	11000
244 SEP 1	004122	31.776	141.726	33	5.5	5.7	SOUTH OF HONSHU, JAPAN.	11000
244 SEP 1	114833	-4.303	102.648	32	5.8	5.2	SOUTHERN SUMATERA, INDONESIA.	11000
244 SEP 1	140319	2.952	96.188	33	5.9	6.3	NORTHERN SUMATERA, INDONESIA.	11000
246 SEP 3	031603	14.365	-92.669	33	5.4	5.1	NEAR COAST OF CHIAPAS, MEXICO	11000
246 SEP 3	123502	14.627	-92.865	33	5.8	6.7	NEAR COAST OF CHIAPAS, MEXICO.	11000
247 SEP 4	113839	36.401	70.872	200	6.0		HINDU KUSH REGION, AFGHANISTAN.	11000
247 SEP 4	213933	-9.672	122.514	33	5.8	5.8	SAVU SEA.	11000
249 SEP 6	035558	-4.654	153.253	33	6.0	6.6	NEW IRELAND REGION, P.N.G.	11000
250 SEP 7	024854	-31.558	-179.494	33	5.7	6.5	KERMADEC ISLANDS REGION.	11000
251 SEP 8	113838	30.177	52.107	25	4.9	4.3	Northern Iran	11010
251 SEP 8	195438	40.120	52.180	33	4.5		TURKMENISTAN	11010
253 SEP 10	150439	39.135	144.369	33	4.6		OFF EAST COAST OF HONSHU, JAPAN	11010
253 SEP 10	172806	14.548	-92.832	33	5.5	5.3	NEAR COAST OF CHIAPAS, MEXICO.	11010
253 SEP 10	191254	14.713	-92.781	34	6.3	7.2	NEAR COAST OF CHIAPAS, MEXICO.	11010
254 SEP 11	045532	42.060	142.541	53	5.5		HOKKAIDO, JAPAN REGION.	11010
254 SEP 11	173645	20.054	121.465	33	5.3	5.2	PHILIPPINE ISLANDS REGION	10010
255 SEP 12	032239	13.819	-90.628	69	5.6		NEAR COAST OF GUATEMALA.	00010
255 SEP 12	082235	-29.437	-177.291	33	5.5	5.7	KERMADEC ISLANDS, NEW ZEALAND.	00010
256 SEP 13	015300	40.330	35.269	10	3.7		TURKEY.	00010
256 SEP 13	052208	-6.135	149.866	38	5.3	5.6	NEW BRITAIN REGION, P.N.G.	00010
256 SEP 13	123753	-29.502	-177.275	33	5.8	6.1	KERMADEC ISLANDS, NEW ZEALAND.	00010
259 SEP 16	005927	44.499	149.052	39	5.7	5.0	KURIL ISLANDS	10010
261 SEP 18	002746	1.630	126.717	33	5.4	5.2	NORTHERN MOLUCCA SEA	11110
261 SEP 18	050227	36.380	71.645	117	6.2		AFGHANISTAN-TAJIKISTAN BORD REG.	11110
262 SEP 19	041834	-60.053	-26.826	33	5.4	5.3	SOUTH SANDWICH ISLANDS REGION	11010
262 SEP 19	141059	14.545	-93.284	33	5.8	6.3	NEAR COAST OF CHIAPAS, MEXICO.	11010
263 SEP 20	101742	0.760	-29.480	10	5.8	5.9	CENTRAL MID-ATLANTIC RIDGE.	11010
264 SEP 21	032855	42.307	-122.005	11	5.7	5.8	OREGON.	11010

Table 1 (continued)

Date	Origin Time(UTC)	Lat	Lon	Z	Mb	Ms	Event Location	sta 12345
264 SEP 21	185308	-4.621	-105.832	10	5.1	5.2	CEN EAST PACIFIC RISE & ethopia	11010
265 SEP 22	123706	-6.483	154.857	50	6.0	6.0	SOLOMON ISLANDS.	11010
266 SEP 23	200401	78.333	5.632	10	4.7	4.6	SVALBARD REGION	11010
268 SEP 25	044419	38.301	73.169	100	4.5		TAJIKISTAN-XINJIANG BORDER REG.	11010
269 SEP 26	033118	10.359	137.996	33	5.9	6.0	WESTERN CAROLINE ISLANDS.	11010
269 SEP 26	115552	13.560	145.500	33	5.7	5.5	MARIANA ISLANDS.	11010
270 SEP 27	044355	30.745	132.153	39	5.5	5.2	SOUTHEAST OF SHIKOKU, JAPAN	11010
270 SEP 27	133733	-53.674	-51.984	33	6.0	6.4	SOUTH ATLANTIC OCEAN.	11010
271 SEP 28	015211	39.756	20.509	10	3.8		GREECE-ALBANIA BORDER REGION. ML	11010
272 SEP 29	111604	0.527	121.626	109	5.9	5.7	MINAHASSA PENINSULA, SULAWESI.	11000
272 SEP 29	141801	36.350	70.850	192	4.7		HINDU KUSH REGION, AFGHANISTAN	11000
272 SEP 29	182621	-42.534	-18.337	10	5.8	5.9	SOUTHERN MID-ATLANTIC RIDGE	11000
272 SEP 29	222548	18.063	76.444	6	6.3	6.3	SOUTHERN INDIA.	11000
273 SEP 30	170447	11.833	92.556	33	5.4	5.1	ANDAMAN ISLANDS, INDIA	11000
273 SEP 30	182754	15.666	-94.681	33	5.7	6.3	NEAR COAST OF OAXACA, MEXICO.	11000
274 OCT 1	035933	36.606	24.044	88	4.9		SOUTHERN GREECE	11000
275 OCT 2	084235	38.165	88.640	33	6.2	6.3	SOUTHERN XINJIANG, CHINA	10000
275 OCT 2	155404	37.511	140.629	86	5.0		EASTERN HONSHU, JAPAN	10000
276 OCT 3	235412	13.182	145.276	83	5.0		MARIANA ISLANDS.	10000
277 OCT 4	205438	-21.355	-174.266	33	5.7	5.9	TONGA ISLANDS.	10100
278 OCT 5	015956	41.642	89.682	0	5.9	4.8	SOUTHERN XINJIANG, CHINA.	10100
278 OCT 5	050948	-6.107	128.936	33	5.8	6.1	BANDA SEA.	10100
278 OCT 5	212802	77.673	126.281	10	5.1		LAPTEV SEA	10100
280 OCT 7	032702	38.172	88.565	33	5.0		SOUTHERN XINJIANG, CHINA	10000
280 OCT 7	175938	36.468	70.645	217	5.1		HINDU KUSH REGION, AFGHANISTAN	10000
281 OCT 8	182346	46.511	149.990	163	5.4		KURIL ISLANDS	10001
282 OCT 9	222421	11.748	57.548	10	5.0	4.0	ARABIAN SEA	10000
284 OCT 11	130730	-17.659	-178.804	556	5.9		FIJI ISLANDS REGION	10110
284 OCT 11	155422	31.987	137.890	365	6.3		SOUTH OF HONSHU, JAPAN.	10110
285 OCT 12	210452	13.020	51.018	10	5.0		EASTERN GULF OF ADEN	10111
286 OCT 13	005232	7.546	121.535	33	5.2	4.7	MINDANAO, PHILIPPINE ISLANDS	10111
286 OCT 13	020600	-5.909	146.017	24	6.5	7.2	EASTERN NEW GUINEA REG., P.N.G.	10111
286 OCT 13	233421	28.611	103.422	33	4.9		SICHUAN, CHINA	10111
287 OCT 14	120235	-50.235	139.429	10	5.4	5.6	South of Australia	10011
288 OCT 15	223717	40.998	48.293	33	4.6	4.2	Eastern Caucasus	10011
289 OCT 16	030531	-5.964	146.205	33	6.2	6.4	EASTERN NEW GUINEA REG., P.N.G.	10011
289 OCT 16	105225	7.381	123.257	33	5.3	5.5	MINDANAO, PHILIPPINE ISLANDS	10011
290 OCT 17	092301	-7.261	119.753	454	5.2		FLORES SEA	10011
291 OCT 18	124136	38.647	70.206	33	4.6		AFGHANISTAN-TAJIKISTAN BORD REG.	10011
291 OCT 18	135713	22.127	62.688	10	5.4	4.6	ARABIAN SEA	10011
291 OCT 18	205113	28.770	34.780	10	4.7		EGYPT	10011
292 OCT 19	040223	-22.110	-65.928	279	5.8		JUJUY PROVINCE, ARGENTINA.	10011
292 OCT 19	153136	38.630	73.540	33	4.8		TAJIKISTAN-XINJIANG BORDER REG.	10011
294 OCT 21	073655	-54.474	-139.040	10	5.4	5.7	Pacific Antartic Ridge	10011
294 OCT 21	215223	30.152	51.175	33	5.1		NORTHERN IRAN	10111
295 OCT 22	084216	-54.684	-26.375	33	5.5	5.4	SOUTH SANDWICH ISLANDS REGION	10111
297 OCT 24	055329	11.300	125.375	49	5.5	5.2	SAMAR, PHILIPPINE ISLANDS	10011
297 OCT 24	075217	16.858	-98.604	33	6.1	6.6	NEAR COAST OF GUERRERO, MEXICO.	10011
297 OCT 24	153608	-55.638	-128.064	10	5.2	5.5	PACIFIC-ANTARCTIC RIDGE	10011
298 OCT 25	100713	-5.908	145.956	33	5.6		EASTERN NEW GUINEA REG., P.N.G.	10001

Table 1 (continued)

Date	Origin Time(UTC)	Lat	Lon	Z	Mb	Ms	Event Location	sta 12345
298 OCT 25	102704	-5.914	145.986	33	6.3	7.1	EASTERN NEW GUINEA REG., P.N.G.	10011
298 OCT 25	143320	41.498	49.600	33	4.1		Caspain Sea	10011
299 OCT 26	113825	38.441	98.649	33	5.8	5.4	Qinghai, China	10011
301 OCT 28	015206	41.568	142.102	70	5.1		HOKKAIDO, JAPAN REGION	10111
302 OCT 29	040905	51.552	-178.169	34	5.8	5.3	ANDREANOF ISLANDS, ALEUTIAN IS.	10111
303 OCT 30	083033	15.340	121.740	33	5.3	5.1	LUZON, PHILIPPINE ISLANDS	10111
303 OCT 30	175903	-31.609	-68.245	110	6.0		SAN JUAN PROVINCE, ARGENTINA.	10111
303 OCT 30	230553	30.320	67.640	10	4.7		PAKISTAN.	10111
306 NOV 2	071448	42.975	130.930	517	4.8		E. RUSSIA-N.E. CHINA BORDER REG.	10111
307 NOV 3	131810	-7.219	67.903	10	5.5	5.4	Mid-Indian Ridge	10111
307 NOV 3	183933	28.674	34.681	14	4.9		Egypt, Note 5.3 in NewGuinea	10111
308 NOV 4	051836	38.371	21.984	10	5.2	5.2	GREECE.	10111
309 NOV 5	070209	-6.940	106.316	107	5.2		JAWA, INDONESIA.	10111
309 NOV 5	223720	-3.053	148.132	9	5.6	6.2	BISMARCK SEA	10111
312 NOV 8	010602	28.673	34.668	10	5.0		EGYPT.	10111
312 NOV 8	204854	36.186	141.734	33	5.3	4.7	NEAR EAST COAST OF HONSHU, JAPAN	10111
313 NOV 9	021403	14.242	53.712	10	5.4	5.1	ARABIAN SEA	10111
314 NOV 10	214500	-22.381	179.085	600	5.3		SOUTH OF FIJI ISLANDS	10111
315 NOV 11	002835	50.253	-177.417	33	6.3	5.6	ANDREANOF ISLANDS, ALEUTIAN IS.	10111
315 NOV 11	101400	-4.552	153.021	89	5.4	5.5	NEW IRELAND REGION, P.N.G.	10111
316 NOV 12	111633	51.342	-177.925	33	5.1	5.0	Andraenof Islands	10111
317 NOV 13	001648	16.448	-98.644	10	5.9	5.3	NEAR COAST OF GUERRERO, MEXICO.	10111
317 NOV 13	011805	51.916	158.740	47	6.5	7.1	NEAR EAST COAST OF KAMCHATKA.	10111
319 NOV 15	224516	-18.550	167.720	33	5.2	5.0	VANUATU ISLANDS	10110
320 NOV 16	155249	30.748	67.280	33	5.5	5.6	PAKISTAN.	10110
321 NOV 17	111853	51.797	158.767	45	6.1	5.5	NEAR EAST COAST OF KAMCHATKA.	10110
323 NOV 19	014323	54.399	-164.238	33	6.1	6.2	UNIMAK ISLAND REGION.	10110
323 NOV 19	090539	7.368	-34.712	10	5.6	5.6	CENTRAL MID-ATLANTIC RIDGE	10110
324 NOV 20	192451	60.147	-153.077	122	5.3		SOUTHERN ALASKA.	10110
326 NOV 22	030102	5.785	126.495	100	5.7		MINDANAO, PHILIPPINE ISLANDS	10111
329 NOV 25	083114	-22.005	170.128	33	5.7	5.6	LOYALTY ISLANDS REGION.	10111
329 NOV 25	202400	-0.965	-13.200	10	5.7	5.5	NORTH OF ASCENSION ISLAND.	10111
330 NOV 26	232006	-9.526	158.038	33	5.6	6.2	SOLOMON ISLANDS.	10111
331 NOV 27	061123	38.597	141.224	108	5.9		NEAR EAST COAST OF HONSHU,	10111
332 NOV 28	105027	-5.617	110.276	566	5.5		JAVA SEA	10111
332 NOV 28	205926	36.463	71.330	108	5.1		AFGHANISTAN-TAJIKISTAN BORD REG.	10111
333 NOV 29	202842	10.240	126.468	33	5.3	5.7	PHILIPPINE ISLANDS REGION	10111
334 NOV 30	045926	-59.138	-18.138	33	5.2	5.5	SOUTH WESTERN ATLANTIC	10111
334 NOV 30	203714	39.266	75.515	33	5.1	5.6	SOUTHERN XINJIANG, CHINA.	10111
335 DEC 1	005901	-57.369	-25.406	33	5.7	5.3	SOUTH SANDWICH ISLANDS REGION	10111
336 DEC 2	143916	36.548	70.500	200	4.9		HINDU KUSH REGION, AFGHANISTAN	10111
337 DEC 3	054107	51.222	179.264	33	5.2	5.0	RAT ISLANDS, ALEUTIAN ISLANDS.	10111
337 DEC 3	123628	-60.350	-20.190	33	5.3	5.2	SOUTHWESTERN ATLANTIC OCEAN	10111
340 DEC 6	104204	-6.325	154.902	48	5.6	5.8	SOLOMON ISLANDS.	10100
340 DEC 6	205443	6.744	78.664	10	5.5		LACCADIVE SEA.	10100
343 DEC 9	043222	0.497	125.982	33	6.3	6.7	Northern Molucca Sea	10100
343 DEC 9	113830	0.426	125.890	33	6.1	6.4	Northern Molucca Sea	10100
344 DEC 10	085938	20.809	121.271	33	5.8	5.8	PHILIPPINE ISLANDS REGION.	10100

References

Ammon, C. J., The isolation of receiver effects from teleseismic P waveforms, *Bull. Seism . Soc. Am..*, **81**, 2504-2510, 1991.

Ammon, C. J., G. E. Randall and G. Zandt, On the resolution and non-uniqueness of receiver function inversions, *J. Geophys. Res.*, **95**, 15303-15318, 1990.

Berberian, M., The southern Caspian: A compressional depression floored by trapped, modified oceanic crust, *Can. J. Earth Sci.*, **20**, 163-183, 1983.

Berberian, M. and G. C. P. King, Towards a paleogeography and tectonic evolution of Iran, *Can. J. Earth Sci.*, **18**, 210-265, 1981.

Berger, J., D. C. Agnew, R. L. Parker and W. E. Farrell, Seismic system calibration: 2. Cross-spectral calibration using random binary signals, *Bull. Seism.. Soc. Am.*, **69**, 271-288, 1979.

Glibkin, M., *The Atlas of Mud Volcanoes of the Azerbaijan SSR*, Publishing house of the Academy of Sciences of the Azerbaijan, SSR, Baku, 1971, (in Russian).

Jackson, J. A., and D. McKenzie, Active tectonics of the Alpine-Himalayan Belt between western Turkey and Pakistan, *Geophys. J. R. Astr. Soc.*, **77**, 185-264, 1984.

Kadinsky-Cade, K., M. Barazangi, J. Oliver, and B. Isacks, Lateral variations of high-frequency seismic wave propagation at regional distances across the Turkish and Iranian Plateaus, *J. Geophys. Res.*, **86**, 9377-9369, 1981.

Langston, C. A., The effect of planer dipping structure on source and receiver responses for constant ray parameter, *Bull. Seism.. Soc. Am.*, **67**, 713-724, 1977.

Langston, C. A., Structure under Mount Rainier, Washington inferred from teleseismic body waves, *J. Geophys. Res.*, **84**, 4749-4762, 1979.

Mangino, S. G., and J. E. Ebel, The receiver structure beneath the Chinese digital seismograph network (CDSN) stations: Preliminary results, *PL-TR-92-2149*, Phillips Laboratory, Hanscom AFB, MA, 1992. **ADA256681**

Mangino, S. G., G. Zandt and C. J. Ammon, The receiver structure beneath Mina, Nevada, *Bull. Seism.. Soc. Am.*, **83**, 542-560, 1993.

Neprochnov, Y. P., Structure of the earth's crust of epi-continental seas: Caspian, Black, and Mediterranean, *Can. J. Earth Sci.*, **5**, 1037-1043, 1968.

Owens, T. J., and R. S. Crosson, Shallow Structure effects on Broadband Teleseismic P Waveforms, *Bull. Seism.. Soc. Am.*, **78**, 96-108, 1988.

Priestley, K., C. Baker and J. Jackson, Implications of earthquake focal mechanism data for the active tectonics of the south Caspian Basin and surrounding regions, *Geophys. J. Int.*, (in press), 1994.

Rezanov, I. A. and S. S. Chamo, Reasons for absence of a 'granitic' layer in basins of the South Caspian and Black Sea type, *Can. J. Earth Sci.*, **6**, 671-678, 1969.

Tapley, W. C. and J. E. Tull, *SAC-Seismic Analysis Code*, Lawrence Livermore National Laboratory, Mail Stop L-205, Livermore, CA, 1991.

Prof. Thomas Ahrens
Seismological Lab, 252-21
Division of Geological & Planetary Sciences
California Institute of Technology
Pasadena, CA 91125

Prof. Keiiti Aki
Center for Earth Sciences
University of Southern California
University Park
Los Angeles, CA 90089-0741

Prof. Shelton Alexander
Geosciences Department
403 Deike Building
The Pennsylvania State University
University Park, PA 16802

Prof. Charles B. Archambeau
CIRES
University of Colorado
Boulder, CO 80309

Dr. Thomas C. Bache, Jr.
Science Applications Int'l Corp.
10260 Campus Point Drive
San Diego, CA 92121 (2 copies)

Prof. Muawia Barazangi
Cornell University
Institute for the Study of the Continent
3126 SNEE Hall
Ithaca, NY 14853

Dr. Jeff Barker
Department of Geological Sciences
State University of New York
at Binghamton
Vestal, NY 13901

Dr. Douglas R. Baumgardt
ENSCO, Inc
5400 Port Royal Road
Springfield, VA 22151-2388

Dr. Susan Beck
Department of Geosciences
Building #77
University of Arizona
Tuscon, AZ 85721

Dr. T.J. Bennett
S-CUBED
A Division of Maxwell Laboratories
11800 Sunrise Valley Drive, Suite 1212
Reston, VA 22091

Dr. Robert Blandford
AFTAC/TT, Center for Seismic Studies
1300 North 17th Street
Suite 1450
Arlington, VA 22209-2308

Dr. Stephen Bratt
ARPA/NMRO
3701 North Fairfax Drive
Arlington, VA 22203-1714

Dale Breding
U.S. Department of Energy
Recipient, IS-20, GA-033
Office of Arms Control
Washington, DC 20585

Dr. Lawrence Burdick
IGPP, A-025
Scripps Institute of Oceanography
University of California, San Diego
La Jolla, CA 92093

Dr. Robert Burridge
Schlumberger-Doll Research Center
Old Quarry Road
Ridgefield, CT 06877

Dr. Jerry Carter
Center for Seismic Studies
1300 North 17th Street
Suite 1450
Arlington, VA 22209-2308

Dr. Martin Chapman
Department of Geological Sciences
Virginia Polytechnical Institute
21044 Derring Hall
Blacksburg, VA 24061

Mr Robert Cockerham
Arms Control & Disarmament Agency
320 21st Street North West
Room 5741
Washington, DC 20451,

Prof. Vernon F. Cormier
Department of Geology & Geophysics
U-45, Room 207
University of Connecticut
Storrs, CT 06268

Prof. Steven Day
Department of Geological Sciences
San Diego State University
San Diego, CA 92182

Dr. Zoltan Der
ENSCO, Inc.
5400 Port Royal Road
Springfield, VA 22151-2388

Prof. Adam Dziewonski
Hoffman Laboratory, Harvard University
Dept. of Earth Atmos. & Planetary Sciences
20 Oxford Street
Cambridge, MA 02138

Prof. John Ebel
Department of Geology & Geophysics
Boston College
Chestnut Hill, MA 02167

Eric Fielding
SNEE Hall
INSTOC
Cornell University
Ithaca, NY 14853

Dr. Petr Firbas
Institute of Physics of the Earth
Masaryk University Brno
Jecna 29a
612 46 Brno, Czech Republic

Dr. Mark D. Fisk
Mission Research Corporation
735 State Street
P.O. Drawer 719
Santa Barbara, CA 93102

Prof. Donald Forsyth
Department of Geological Sciences
Brown University
Providence, RI 02912

Dr. Cliff Frolich
Institute of Geophysics
8701 North Mopac
Austin, TX 78759

Dr. Holly Given
IGPP, A-025
Scripps Institute of Oceanography
University of California, San Diego
La Jolla, CA 92093

Dr. Jeffrey W. Given
SAIC
10260 Campus Point Drive
San Diego, CA 92121

Dr. Dale Glover
Defense Intelligence Agency
ATTN: ODT-1B
Washington, DC 20301

Dan N. Hagedon
Pacific Northwest Laboratories
Battelle Boulevard
Richland, WA 99352

Dr. James Hannon
Lawrence Livermore National Laboratory
P.O. Box 808
L-205
Livermore, CA 94550

Prof. David G. Harkrider
Seismological Laboratory
Division of Geological & Planetary Sciences
California Institute of Technology
Pasadena, CA 91125

Prof. Danny Harvey
CIRES
University of Colorado
Boulder, CO 80309

Prof. Donald V. Helmberger
Seismological Laboratory
Division of Geological & Planetary Sciences
California Institute of Technology
Pasadena, CA 91125

Prof. Eugene Herrin
Institute for the Study of Earth and Man
Geophysical Laboratory
Southern Methodist University
Dallas, TX 75275

Prof. Robert B. Herrmann
Department of Earth & Atmospheric Sciences
St. Louis University
St. Louis, MO 63156

Prof. Lane R. Johnson
Seismographic Station
University of California
Berkeley, CA 94720

Prof. Thomas H. Jordan
Department of Earth, Atmospheric &
Planetary Sciences
Massachusetts Institute of Technology
Cambridge, MA 02139

Prof. Alan Kafka
Department of Geology & Geophysics
Boston College
Chestnut Hill, MA 02167

Robert C. Kemerait
ENSCO, Inc.
445 Pineda Court
Melbourne, FL 32940

Dr. Karl Koch
Institute for the Study of Earth and Man
Geophysical Laboratory
Southern Methodist University
Dallas, Tx 75275

U.S. Dept of Energy
Max Koontz, NN-20, GA-033
Office of Research and Develop.
1000 Independence Avenue
Washington, DC 20585

Dr. Richard LaCoss
MIT Lincoln Laboratory, M-200B
P.O. Box 73
Lexington, MA 02173-0073

Dr. Fred K. Lamb
University of Illinois at Urbana-Champaign
Department of Physics
1110 West Green Street
Urbana, IL 61801

Prof. Charles A. Langston
Geosciences Department
403 Deike Building
The Pennsylvania State University
University Park, PA 16802

Jim Lawson, Chief Geophysicist
Oklahoma Geological Survey
Oklahoma Geophysical Observatory
P.O. Box 8
Leonard, OK 74043-0008

Prof. Thorne Lay
Institute of Tectonics
Earth Science Board
University of California, Santa Cruz
Santa Cruz, CA 95064

Dr. William Leith
U.S. Geological Survey
Mail Stop 928
Reston, VA 22092

Mr. James F. Lewkowicz
Phillips Laboratory/GPEH
29 Randolph Road
Hanscom AFB, MA 01731-3010(2 copies)

Mr. Alfred Lieberman
ACDA/VI-OA State Department Building
Room 5726
320-21st Street, NW
Washington, DC 20451

Prof. L. Timothy Long
School of Geophysical Sciences
Georgia Institute of Technology
Atlanta, GA 30332

Dr. Randolph Martin, III
New England Research, Inc.
76 Olcott Drive
White River Junction, VT 05001

Dr. Robert Masse
Denver Federal Building
Box 25046, Mail Stop 967
Denver, CO 80225

Dr. Gary McCartor
Department of Physics
Southern Methodist University
Dallas, TX 75275

Prof. Thomas V. McEvilly
Seismographic Station
University of California
Berkeley, CA 94720

Dr. Art McGarr
U.S. Geological Survey
Mail Stop 977
U.S. Geological Survey
Menlo Park, CA 94025

Dr. Keith L. McLaughlin
S-CUBED
A Division of Maxwell Laboratory
P.O. Box 1620
La Jolla, CA 92038-1620

Stephen Miller & Dr. Alexander Florence
SRI International
333 Ravenswood Avenue
Box AF 116
Menlo Park, CA 94025-3493

Prof. Bernard Minster
IGPP, A-025
Scripps Institute of Oceanography
University of California, San Diego
La Jolla, CA 92093

Prof. Brian J. Mitchell
Department of Earth & Atmospheric Sciences
St. Louis University
St. Louis, MO 63156

Mr. Jack Murphy
S-CUBED
A Division of Maxwell Laboratory
11800 Sunrise Valley Drive, Suite 1212
Reston, VA 22091 (2 Copies)

Dr. Keith K. Nakanishi
Lawrence Livermore National Laboratory
L-025
P.O. Box 808
Livermore, CA 94550

Prof. John A. Orcutt
IGPP, A-025
Scripps Institute of Oceanography
University of California, San Diego
La Jolla, CA 92093

Prof. Jeffrey Park
Kline Geology Laboratory
P.O. Box 6666
New Haven, CT 06511-8130

Dr. Howard Patton
Lawrence Livermore National Laboratory
L-025
P.O. Box 808
Livermore, CA 94550

Dr. Frank Pilotte
HQ AFTAC/TT
1030 South Highway A1A
Patrick AFB, FL 32925-3002

Dr. Jay J. Pulli
Radix Systems, Inc.
201 Perry Parkway
Gaithersburg, MD 20877

Dr. Robert Reinke
ATTN: FCTVTD
Field Command
Defense Nuclear Agency
Kirtland AFB, NM 87115

Prof. Paul G. Richards
Lamont-Doherty Geological Observatory
of Columbia University
Palisades, NY 10964

Mr. Wilmer Rivers
Teledyne Geotech
314 Montgomery Street
Alexandria, VA 22314

Dr. Alan S. Ryall, Jr.
ARPA/NMRO
3701 North Fairfax Drive
Arlington, VA 22203-1714

Dr.Chandan K. Saikia
Woodward Clyde- Consultants
566 El Dorado Street
Pasadena, CA 91101

Dr. Richard Sailor
TASC, Inc.
55 Walkers Brook Drive
Reading, MA 01867

Prof. Charles G. Sammis
Center for Earth Sciences
University of Southern California
University Park
Los Angeles, CA 90089-0741

Prof. Christopher H. Scholz
Lamont-Doherty Geological Observatory
of Columbia University
Palisades, NY 10964

Dr. Susan Schwartz
Institute of Tectonics
1156 High Street
Santa Cruz, CA 95064

Secretary of the Air Force
(SAFRD)
Washington, DC 20330

Office of the Secretary of Defense
DDR&E
Washington, DC 20330

Thomas J. Sereno, Jr.
Science Application Int'l Corp.
10260 Campus Point Drive
San Diego, CA 92121

Dr. Michael Shore
Defense Nuclear Agency/SPSS
6801 Telegraph Road
Alexandria, VA 22310

Dr. Robert Shumway
University of California Davis
Division of Statistics
Davis, CA 95616

Dr. Matthew Sibol
Virginia Tech
Seismological Observatory
4044 Derring Hall
Blacksburg, VA 24061-0420

Prof. David G. Simpson
IRIS, Inc.
1616 North Fort Myer Drive
Suite 1050
Arlington, VA 22209

Donald L. Springer
Lawrence Livermore National Laboratory
L-025
P.O. Box 808
Livermore, CA 94550

Dr. Jeffrey Stevens
S-CUBED
A Division of Maxwell Laboratory
P.O. Box 1620
La Jolla, CA 92038-1620

Lt. Col. Jim Stobie
ATTN: AFOSR/NL
110 Duncan Avenue
Bolling AFB
Washington, DC 20332-0001

Prof. Brian Stump
Los Alamos National Laboratory
EES-3
Mail Stop C-335
Los Alamos, NM 87545

Prof. Jeremiah Sullivan
University of Illinois at Urbana-Champaign
Department of Physics
1110 West Green Street
Urbana, IL 61801

Prof. L. Sykes
Lamont-Doherty Geological Observatory
of Columbia University
Palisades, NY 10964

Dr. David Taylor
ENSCO, Inc.
445 Pineda Court
Melbourne, FL 32940

Dr. Steven R. Taylor
Los Alamos National Laboratory
P.O. Box 1663
Mail Stop C335
Los Alamos, NM 87545

Prof. Clifford Thurber
University of Wisconsin-Madison
Department of Geology & Geophysics
1215 West Dayton Street
Madison, WS 53706

Prof. M. Nafi Toksoz
Earth Resources Lab
Massachusetts Institute of Technology
42 Carleton Street
Cambridge, MA 02142

Dr. Larry Turnbull
CIA-OSWR/NED
Washington, DC 20505

Dr. Gregory van der Vink
IRIS, Inc.
1616 North Fort Myer Drive
Suite 1050
Arlington, VA 22209

Dr. Karl Veith
EG&G
5211 Auth Road
Suite 240
Suitland, MD 20746

Prof. Terry C. Wallace
Department of Geosciences
Building #77
University of Arizona
Tuscon, AZ 85721

Dr. Thomas Weaver
Los Alamos National Laboratory
P.O. Box 1663
Mail Stop C335
Los Alamos, NM 87545

Dr. William Wortman
Mission Research Corporation
8560 Cinderbed Road
Suite 700
Newington, VA 22122

Prof. Francis T. Wu
Department of Geological Sciences
State University of New York
at Binghamton
Vestal, NY 13901

Prof Ru-Shan Wu
University of California, Santa Cruz
Earth Sciences Department
Santa Cruz
, CA 95064

ARPA, OASB/Library
3701 North Fairfax Drive
Arlington, VA 22203-1714

HQ DNA
ATTN: Technical Library
Washington, DC 20305

Defense Intelligence Agency
Directorate for Scientific & Technical Intelligence
ATTN: DTIB
Washington, DC 20340-6158

Defense Technical Information Center
Cameron Station
Alexandria, VA 22314 (2 Copies)

TACTEC
Battelle Memorial Institute
505 King Avenue
Columbus, OH 43201 (Final Report)

Phillips Laboratory
ATTN: XPG
29 Randolph Road
Hanscom AFB, MA 01731-3010

Phillips Laboratory
ATTN: GPE
29 Randolph Road
Hanscom AFB, MA 01731-3010

Phillips Laboratory
ATTN: TSML
5 Wright Street
Hanscom AFB, MA 01731-3004

Phillips Laboratory
ATTN: PL/SUL
3550 Aberdeen Ave SE
Kirtland, NM 87117-5776 (2 copies)

Dr. Michel Bouchon
I.R.I.G.M.-B.P. 68
38402 St. Martin D'Heres
Cedex, FRANCE

Dr. Michel Campillo
Observatoire de Grenoble
I.R.I.G.M.-B.P. 53
38041 Grenoble, FRANCE

Dr. Kin Yip Chun
Geophysics Division
Physics Department
University of Toronto
Ontario, CANADA

Prof. Hans-Peter Harjes
Institute for Geophysic
Ruhr University/Bochum
P.O. Box 102148
4630 Bochum 1, GERMANY

Prof. Eystein Husebye
NTNF/NORSAR
P.O. Box 51
N-2007 Kjeller, NORWAY

David Jepsen
Acting Head, Nuclear Monitoring Section
Bureau of Mineral Resources
Geology and Geophysics
G.P.O. Box 378, Canberra, AUSTRALIA

Ms. Eva Johannisson
Senior Research Officer
FOA
S-172 90 Sundbyberg, SWEDEN

Dr. Peter Marshall
Procurement Executive
Ministry of Defense
Blacknest, Brimpton
Reading FG7-FRS, UNITED KINGDOM

Dr. Bernard Massinon, Dr. Pierre Mechler
Societe Radiomana
27 rue Claude Bernard
75005 Paris, FRANCE (2 Copies)

Dr. Svein Mykkeltveit
NTNT/NORSAR
P.O. Box 51
N-2007 Kjeller, NORWAY (3 Copies)

Prof. Keith Priestley
University of Cambridge
Bullard Labs, Dept. of Earth Sciences
Madingley Rise, Madingley Road
Cambridge CB3 OEZ, ENGLAND

Dr. Jorg Schlittenhardt
Federal Institute for Geosciences & Nat'l Res.
Postfach 510153
D-30631 Hannover , GERMANY

Dr. Johannes Schweitzer
Institute of Geophysics
Ruhr University/Bochum
P.O. Box 1102148
4360 Bochum 1, GERMANY

Trust & Verify
VERTIC
Carrara House
20 Embankment Place
London WC2N 6NN, ENGLAND